# NUMERICAL ANALYSIS AND VERIFICATION OF A PASSIVE RADAR ANTENNA

S. Orasch*, H. Flühr*, P. Ortner*, W. Stocksreiter†, R. Findenig†
* FH JOANNEUM, Institute of Luftfahrt/Aviation, Alte Poststraße 149, 8020 Graz, Austria
† FH JOANNEUM, Institute of Electronic Engineering, Werk-VI-Straße 46, 8605 Kapfenberg, Austria

**Abstract**

Numerical analyses offer the possibility of computing antenna characteristics such as radiation patterns without the need for complex measurement methods. An exact knowledge about the radiation pattern is required to estimate and simulate the coverage of a passive radar system. A log-periodic dipole antenna (LPDA) is commonly employed in passive radar because of its broadband characteristics. This paper proposes a numerical simulation to obtain fundamental antenna parameters by MATLAB. A practical antenna measurement is performed to verify the result of the numerical analysis. In order to demonstrate the necessity of exact radiation patterns, the effect of inaccuracies is illustrated by coverage maps. It can be observed that distinct patterns are computed and measured for specific angles. For this reason the simulation model is investigated to show how frequency and angle affect the computation. Finally recommendations for enhancing the meshing and measurement setup are presented to improve the validity of the results.

**Keywords**

Antenna Measurement; Passive Radar; Numerical Simulation

## 1. INTRODUCTION

Antennas come in different forms and shapes depending on the requirements since an universal antenna cannot be designed for any application. Parameters such as frequency, gain, bandwidth or polarization cause constraints hence a trade-off has to be found. In case of passive radar, which receives signals and reflections from an illuminator of opportunity (IOO), a different antenna design is required compared to monostatic radars. Hence the bandwidth of the antenna is required to be larger to cover the entire frequency band. Broadband antennas such as a log periodic dipole antenna (LPDA) are deployed and covered in this paper. Since transmitter and receiver are separated, the position and characteristic of an antenna has an effect on the probability to detect a target. Numerical analyses are performed in MATLAB to estimate the antenna characteristic and coverage of passive radar. Subsequently the numerical computation of the antenna characteristic is verified in a measurement campaign to evaluate its accuracy. A statement about the quality of the simulation is to be made, additionally the effects of the deviations are described.

## 2. ANTENNA THEORY

The task of a radar antenna is to transmit and receive electromagnetic waves which have been reflected by a target. According to the reciprocity theorem the antenna characteristic remains the same independently of the operation mode allowing to apply the proposed measurement method. An antenna characteristic is mainly described by its radiation pattern, beamwidth, directivity, gain and lobes. To compare antennas with each other theoretical concepts are introduced and described. [1] [p. 310] [2] [p. 161]

### 2.1. Theoretical Antenna

First the so-called isotropic antenna is covered which functions as a reference antenna. The isotropic antenna radiates its power on a surface of a sphere hence it has no preferred direction of transmission or reception. Because of the spherically symmetric charge distribution, in reality a theoretical monopole antenna cannot be realized. However this term is still used for $\lambda/4$ - antennas, which do not have a spherically symmetric charge distribution. [2] [p. 158]

If the distance of the charges is increased to an infinitesimally small length $l \ll \lambda/4$ a Hertzian dipole is created. Compared to the previous radiator the power is not distributed equally on a sphere instead it depends on the elevation $\theta$ and azimuth $\phi$. For instance both theoretical concepts are fed by the same power hence they radiate the same power but in different directions. By expanding the length of the dipole to $l = \lambda/2$ a fundamental and realizable antenna is obtained referred to as the $\lambda/2$-dipole. By arranging $\lambda/2$-dipole



doi: 10.25967/610400

in patterns, antenna arrays are obtained which realize directional antennas. [2] [p. 158, 270] [3] [p.182]

### 2.2. Radiation Pattern

According to IEEE (Institute of Electrical and Electronics Engineers) standards for definition of terms for antennas, a radiation pattern is defined as "the spatial distribution of a quantity that characterizes the electromagnetic field generated by an antenna" [4] [p.30].

### 2.3. Beamwidth

The antenna beamwidth describes the angle between the -3 dB power drop of the main lobe in the radiation pattern. Monostatic radars are required to have a small beamwidth to gain angular (azimuth) resolution. However bistatic radar applies ellipsoid intersection to allocate targets allowing much larger beamwidths. [1] [p.13] [4] [p.18] [5]

### 2.4. Gain and Directivity

Based on IEEE, the anntenna gain describes "the ratio of the radiation intensity in a given direction to the radiation intensity that would be produced if the power accepted by the antenna were isotropically radiated" [4] [p.17]. Hence gain is denoted in dBi and related to directivity by the efficiency factor $\eta$ [2] [p.270].

### 2.5. Impedance Matching and Return Loss

According to the maximum power transfer theorem the transmitted power can be maximized if the internal impedance and matches the load impedance otherwise impedance mismatch occurs. As seen in equation (1) the reflection coefficient $\Gamma$ defines how much power is reflected hence not delivered to the antenna. In this case $Z_L$ describes the impedance of the load and $Z_0$ the impedance of the transmission line. If both values match, the reflection coefficient $\Gamma$ becomes zero. The return loss RL is the logarithmic representation of $\Gamma$ in order to visualize simulation and measurement results. Due to the broadband characteristic of the proposed antenna the return loss is obtained for a series of frequencies. [6][p.113]

$$\Gamma = \frac{Z_L - Z_0}{Z_L + Z_0} \tag{1}$$

$$RL = -20log_{10}(\Gamma) \tag{2}$$

### 2.6. Polarisation

Polarization specifies the orientation of the electric field and can be categorized in linear, circular and elliptical polarization. A $\lambda$/2-dipole has a vertical or horizontal linear polarisation depending on the installation of the antenna. A vertical polarisation is proposed in this paper hence both antennas must be orientated properly in the measurement. In addition the correct polarisation is considered for the simulation. [6] [p.41]

### 2.7. Logarithmic Periodic Dipole Antenna

A logarithmic periodic dipole antenna is an antenna array consisting of $\lambda$/2-dipoles which are arranged in a linear array. Its characteristic does not change over a broad range of frequencies because of the periodic design. The transmitted or received frequency defines the active dipole depending on the $\lambda$/2 resonance since all elements are connected with each other [2] [p.325]. A detailed description and design of LPDA is provided by Rothammel [6] [p.614 ff.].

For this purpose the LPDA WS 100 DA from LD Systems is used to benchmark the numerical simulation in MATLAB. As seen in Figure 1 it consists of nine dipoles embedded in dielectric substrate. According to the specifications it holds a bandwidth of 400 MHz up to 900 MHz while providing a maximum gain of 7 dBi. The LPDA has been used in previous passive radar demonstrations hence it is chosen for the measurement [7].


**FIG 1. LD-System WS 100 DA [8]**

## 3. NUMERICAL SIMULATION

Numerical simulations offer a time- and cost efficient method to design and optimize antennas. The proposed simulation can be computed by off-the-shelf technology and offers a user-friendly environment. To determine its accuracy a digital twin is set up subsequently.

### 3.1. Initialisation

To simulate the proposed antenna, MATLAB including the Antenna Toolbox is chosen. The toolbox provides an antenna catalog and contains a printed log-periodic dipole antenna which matches with the LPDA WS 100 DA. Geometric and material parameter are predefined according to the actual antenna. In addition the correct orientation is defined to ensure a V-V (vertical to vertical) polarization. No information about the exact material can be found in the data sheet hence commonly used materials are

implemented. FR4 is used as dielectric medium and copper is selected for the conducting medium with respect to the measured interspace between conductors. The reference impedance $Z_0$ is set to 50 $\Omega$ according to the WS 100 DA data sheet. Figure 2 shows the implementation and includes geometric simplifications such as roundings. Furthermore the longest $\lambda$/2-dipole is truncated by 10 mm because the original model includes a bent dipole which cannot be realized in the simulation model.

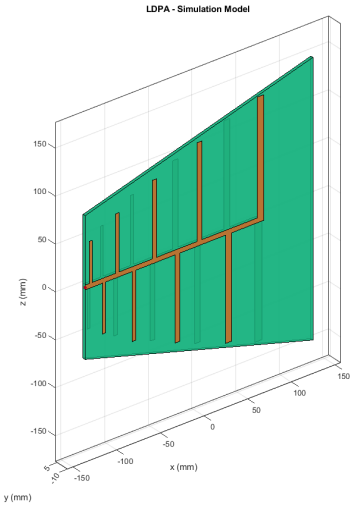


**FIG 2. Simulation Model**

### 3.2. Numerical Method

To estimate the radiation pattern numerically, the method of moments (MOM) is applied by MATLAB. The idea is to define the unknown quantities (surface current, flux density) by known basis functions with unknown coefficients. This allows to set up a linear equation system which can be solved numerically. In principle this problem is described by equation (3) where L defines a linear operator, f the unknown quantities and g the source.

$$L(f) = g \tag{3}$$

The unknown quantities are defined by the product of N weighting coefficients $a_n$ and basis functions $f_n$ as seen in equation (4). By default the Rao-Wilton-Glisson (RWG) basis function is chosen. For discretization surfaces are meshed into triangles and volumes into tetrahedrons. [9]

$$f = \sum_{n=1}^{N} a_n f_n \tag{4}$$

Finally the inner product, also referred to as moment, of the basis function $f_n$ and weighting function $f_m$ is calculated. By demand the moment of the weighting function and residual function converges to zero. Finally a $N \times N$ matrix is obtained allowing to determine the missing coefficients by equation (5). [10][p.43f]

$$\sum_{n=1}^{N} a_n \langle f_m L(f_n) \rangle = \langle f_m, g \rangle \tag{5}$$

### 3.3. Numerical Results

Table 1 provides an overview of all performed computations and measurements. In total six simulations are conducted by simulating the radiation pattern (I-V) at different frequencies and angles. Furthermore the return loss (VI) is computed in form of a frequency sweep for a single angle.

**TAB 1. Simulation and Measuring Overview**

| Nr. | Freq. [MHz] | Azimuth [°] | Elevation [°] | Pol. |
|---|---|---|---|---|
| I | 500 | 0:5:360 | 0 20 45 90 | V-V |
| II | 600 | 0:5:360 | 0 20 45 90 | V-V |
| III | 700 | 0:5:360 | 0 20 45 90 | V-V |
| IV | 800 | 0:5:360 | 0 20 45 90 | V-V |
| V | 900 | 0:5:360 | 0 20 45 90 | V-V |

Figure 3 to Figure 6 plot the numerically computed radiation pattern in Cartesian coordinates. For clarity colors and axis limits are visualized equally.

The simulated return loss is visualized by Figure 7 and includes additional values at the poles of the measured curve. For illustration interpolated values are plotted, in addition the real measured return loss is added to the graph.

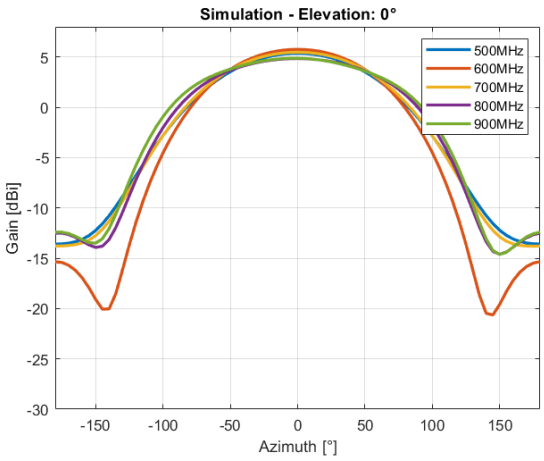


**FIG 3. Simulation - Elevation 0°**

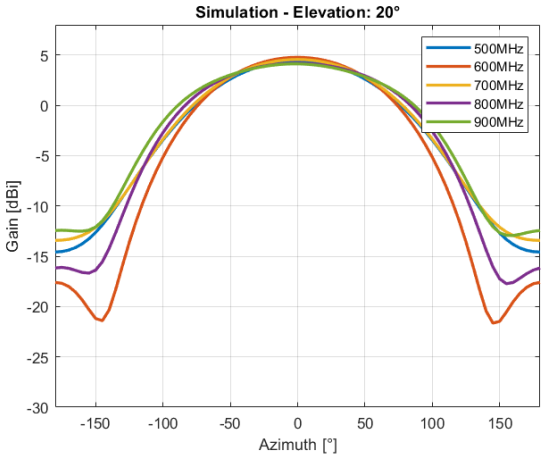


**FIG 4. Simulation - Elevation 20°**

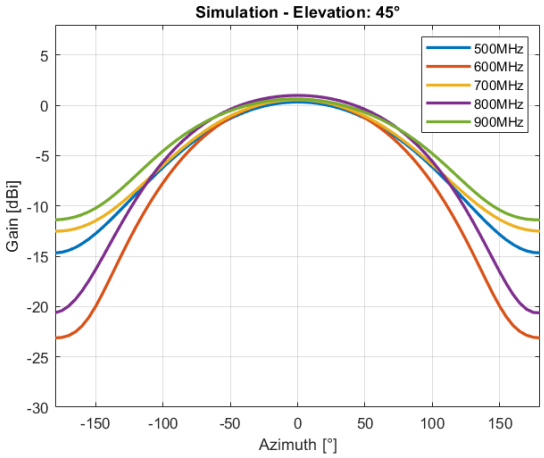


**FIG 5. Simulation - Elevation 45°**

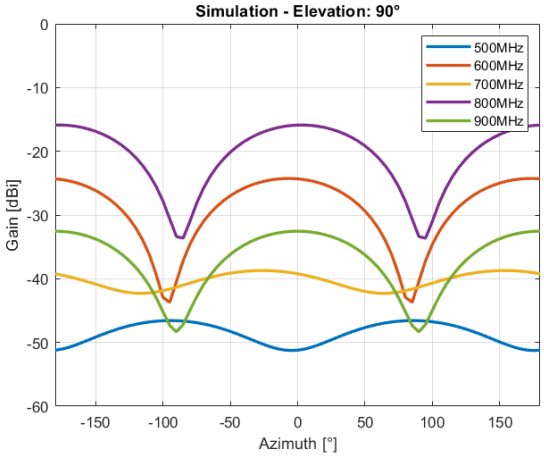


**FIG 6. Simulation - Elevation 90°**

## 4. ANTENNA MEASUREMENT

The measurement was carried out in a rectangular anechoic chamber and follows the concept of measuring far-field radiation described by Yi Huang, Kenneth Chan, Barry Cheeseman [11] and Foegelle [12].

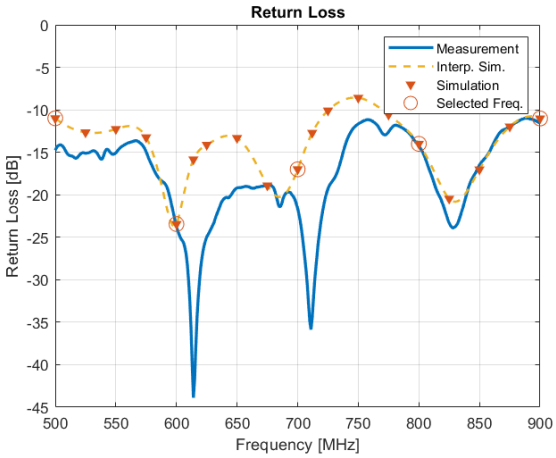


**FIG 7. Simulation and Measurement - Return Loss**

### 4.1. Measurement Setup

In order to perform frequency-domain far-field measurements the far-field the minimum distance $R_{min}$ must be met exceeded to equation (6). It depends on the largest orthogonal antenna component D and the wavelength $\lambda$. For wire type antennas $R_{min}$ should be increased to $10\lambda$. In the actual measurement the distance between both antennas is 2.8 m fulfilling both requirements. [11] [p.2]

$$R_{\text{min}} > \frac{2D^2}{\lambda} \tag{6}$$

To measure the antenna gain two antennas are required namely reference antenna and antenna under test (AUT). At 0 dBm feeding power the AUT radiates a continuous wave (CW) signal which is received by the reference antenna Schwarzbeck BBHA9120E. Due to cable losses at higher frequencies, the output power of the signal generator is increased constantly to ensure constant feeding power. Since the transmitting power $P_{TX}$, the gain of the reference antenna $G_{RX}$ and cable loss $L_C$ including the free space path loss $L_{FSPL}$ is fully known, the transmitter gain $G_{TX}$ can be derived by equation (7). Note that all values are given in dB.

$$G_{\text{TX}} = P_{\text{RX}} - (P_{\text{TX}} + G_{\text{RX}} + L_{\text{C}} + L_{\text{FSPL}}) \tag{7}$$

The Great Circle Method is applied to obtain three-dimensional radiation patterns. Hence the (receiving) reference antenna is fixed vertically pointing to the (transmitting) AUT. If the AUT completes a full azimuthal rotation at a specified elevation angle, a two-dimensional radiation pattern is received. This method has to be repeated for every elevation angle at a given frequency leading to time-consuming measurement. Figure 8 shows both antennas including the remote controlled turntable. Ferrite chocks are used to prevent unwanted cable effects in particular at lower frequencies. For simplification the horizontal-vertical (H-V) radiation pattern is neglected since

preliminary measurements have shown minimal gain below -20 dBi. Because of the broadband characteristic a time-domain far-field measurement has been proposed which can be investigated in further researches. [13] [11] [12]

The return loss is determined by a vector network analyzer which has been calibrated in advance. The antenna mount is connected to a ground plane to avoid interference.

**FIG 8. Reference Antenna Schwarzbeck BBHA9120E *(right)* and AUT LD-Systems WS 100 DA *(left)***

### 4.2. Measurement Results

Figure 9 to Figure 12 illustrate the measured radiation pattern and follow the same layout. All values have been interpolated linearly to improve readability. It must be noted that the turntable rotates clockwisely hence 180° and -180° represent the same value. The measured return loss has been already shown in Figure 7.

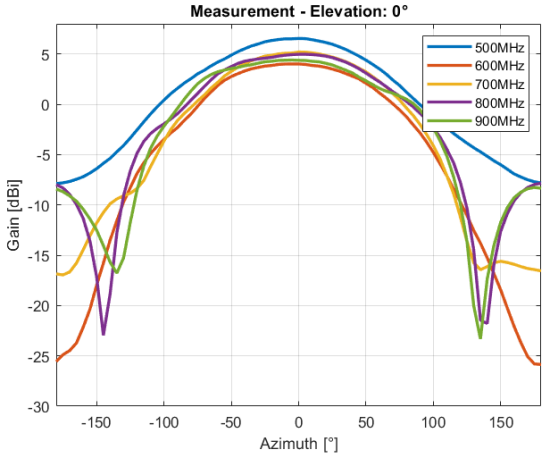


**FIG 9. Measurement - Elevation 0°**

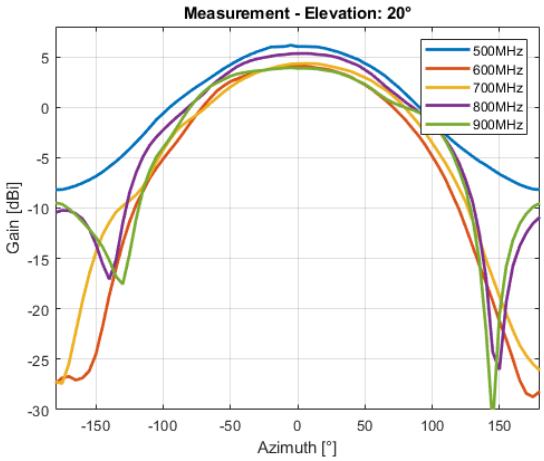


**FIG 10. Measurement - Elevation 20°**

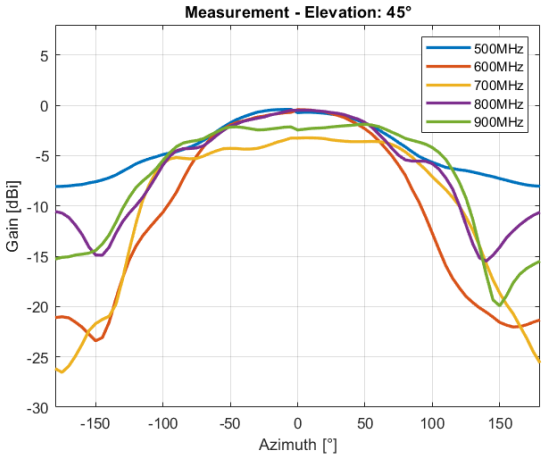


**FIG 11. Measurement - Elevation 45°**

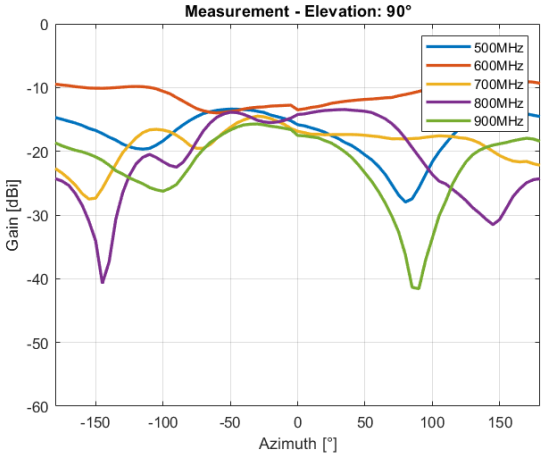


**FIG 12. Measurement - Elevation 90°**

## 5. ANTENNA COVERAGE MAP

In radar design link budget analyses are applied to estimate the received power after taking in account gains and losses. The results can be visualized as a function of range in form of a coverage map. The monostatic radar equation can be modified to derive the passive radar equation by splitting the range $R^4$ into two independent terms $R_{TX}^2 R_{RX}^2$. As seen in equation (8) the received power $P_{RX}$ becomes a function of both ranges if all parameters including the radar cross section (RCS) $\sigma$ are kept constant. Ovals of Cassini are obtained when the range product $R_{TX}^2 R_{RX}^2$ is constant as shown in Figure 13. In practice the received power remains constant independent of whether being near to the transmitter or receiver. The form of the resulting isoline is a function

of the bistatic range and can be open or enclosed. However in case of monostatic radars concentric circles are obtained since transmitter and receiver are identical. [5][p.12]

$$P_{RX} = \frac{P_{TX} G_{TX} G_{RX} \lambda^2 \sigma}{(4\pi)^3 R_{TX}^2 R_{RX}^2} \tag{8}$$

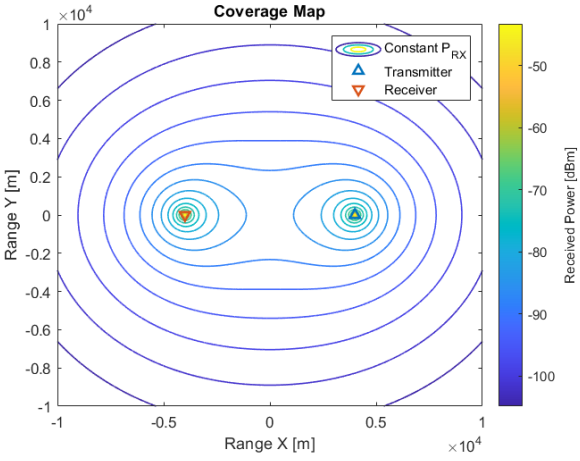


**FIG 13. Ovals of Cassini**

However in reality gain is a function of azimuth and elevation therefore the angle must be considered. To evaluate the effect of radiation patterns on the received power, a multistatic passive radar scenario is set up. One omnidirectional transmitter and three directional receivers are positioned on a flat plain. Although the correct gain is taken into account, many simplifications such as constant RCS and $1/R^2$ propagation is assumed. Furthermore, the frequency is set to 900 MHz and an elevation of 0° is chosen. Note that all receivers point to a common target in the upper left half. To study the effect of radiation patterns an omnidirectional pattern is added to the existing coverage maps.

To avoid accumulating the received power for each receiver, only the maximum value of each cell is selected and displayed. A resolution of 10 $\times$ 10 m is chosen for the computation. Figure 14 shows the heavily simplified coverage map if all receivers share an omnidirectional radiation pattern. Figure 15 and Figure 16 differ only by the radiation pattern obtained in the simulation and measurement.

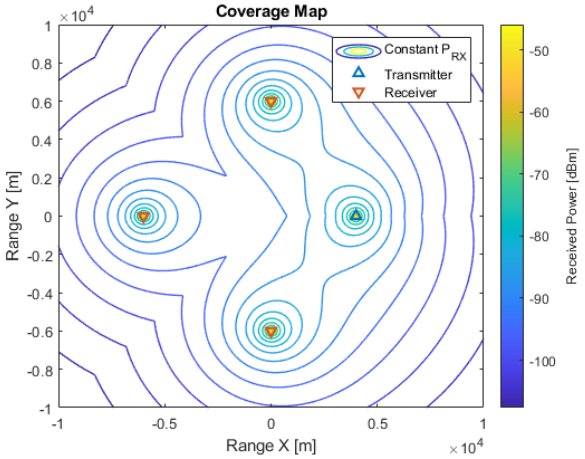


**FIG 14. Omnidirectional - Coverage Map**

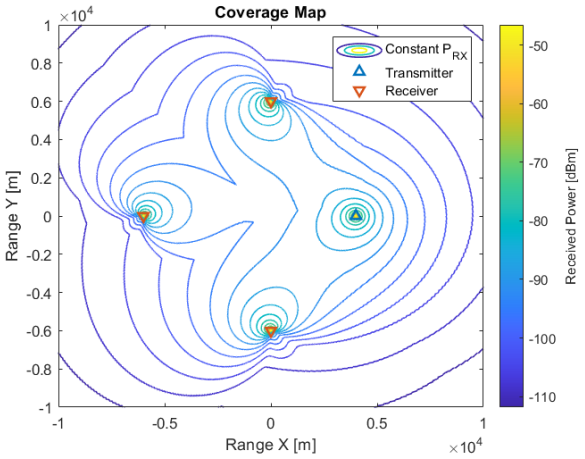


**FIG 15. Simulation - Coverage Map**

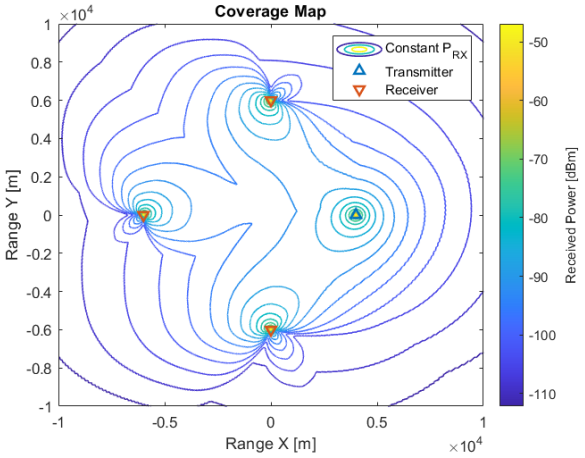


**FIG 16. Measurement - Coverage Map**

## 6. DISCUSSION

In order to assess the results, the accuracy of the simulation is determined using the parameters introduced earlier. Possible model errors or measurement deviations are pointed out and recommendations for improvements are found.

### 6.1. Radiation Pattern

To evaluate the accuracy of the simulation, the plausibility of the obtained lobes is investigated. Table 2 and Table 3 provide a detailed overview about the simulated and measured isotropic gain. Both tables show that the maximum power is radiated/received at an angle of $\theta = 0°$ and $\phi = 0°$ fulfilling the expectation that a single main lobe exists. For a constant eleva-

tion the gain decreases with increasing frequency, since it is assumed that the antenna's transmission line is excited causing it to radiate. This potential effect can be also identified in the simulation results. In both cases the back lobe does not follow a clear trend since it heavily depends on the frequency. However at $\theta = 90°$ distinct deviations occur because in theory a dipole does not emit power at $\theta = 90°$ causing a very low gain in the simulation model. For the measurement it is presumed that the absorption properties of the anechoic chamber are enhanced at higher frequencies resulting in a lower gain for higher frequencies at $\theta = 90°$. Although main and back lobes are reproduced in a convenient way nulls (i.e. directions where almost no power is radiated) are underestimated by the numerical computation. Especially at higher frequencies nulls are observed which occur at $\phi \approx \pm 150°$. The effect of nulls can be clearly identified in the coverage map. All simulated radiation patterns are comparable to the actual results expect for $\theta = 90°$ because of the divergent gain.

By defining an acceptable variance of 1 dBi both gains are compared. In case of elevations $\theta \leq 20°$ reasonable results are obtained although lower frequencies tend to vary. For elevations $\theta \geq 45°$ outliers are measured however no reason for the deviation can be given.

**TAB 2. Simulated Main Lobe and Back Lobe**

| Freq./Ele. | 0° | 20° |
|---|---|---|
| 500 MHz | 5.36,-13.59 | 4.42,-14.58 |
| 600 MHz | 5.76,-15.35 | 4.78,-17.60 |
| 700 MHz | 5.48,-13.80 | 4.56,-13.43 |
| 800 MHz | 4.88,-12.51 | 4.18,-16.16 |
| 900 MHz | 4.85,-12.41 | 4.12,-12.44 |
| **Freq/Ele.** | **45°** | **90°** |
| 500 MHz | 0.33,-14.67 | -51.21 |
| 600 MHz | 0.60,-23.12 | -24.32 |
| 700 MHz | 0.56,-12.51 | -39.22 |
| 800 MHz | 0.63,-20.62 | -15.89 |
| 900 MHz | 0.99,-11.38 | -32.53 |

### 6.2. Beamwidth

It can be shown the simulated and measured beamwidth match on the basis of Table 4 and 5. All values are rounded according to the step size of the azimuth. For $\theta = 90°$ no value is given since no distinct main lobe is received by the radiation pattern. In both cases the beamwidth spreads by increasing the elevation and frequency. However the last two measured frequencies at an elevation $\theta = 45°$ are an exception to this observation. This result is counter-intuitive because generally higher frequencies cause a narrower beamwidth. It is assumed that higher frequencies cause less resonance in the remaining larger dipoles hence no interference is achieved reducing directivity. For fixed elevation a single dipole has constant gain because of the doughnut shaped radiation pattern. On this account it is suggested to analyze the current distribution of the LPDA to clarify the values.

**TAB 3. Measured Main Lobe and Back Lobe**

| Freq./Ele. | 0° | 20° |
|---|---|---|
| 500 MHz | 6.54,-7.88 | 6.02,-8.18 |
| 600 MHz | 4.01,-25.56 | 4.07,-27.33 |
| 700 MHz | 5.20,-16.85 | 4.31,-27.22 |
| 800 MHz | 4.97,-7.97 | 5.33,-10.44 |
| 900 MHz | 4.37,-8.42 | 3.86,-9.52 |
| **Freq/Ele.** | **45°** | **90°** |
| 500 MHz | -0.73,-8.08 | -15.83 |
| 600 MHz | -0.43,-21.09 | -13.50 |
| 700 MHz | -3.27,-26.16 | -16.86 |
| 800 MHz | -0.49,-10.55 | -14.23 |
| 900 MHz | -2.45,-15.27 | -17.51 |

**TAB 4. Simulated Beamwidth**

| Freq./Ele. | 0° | 20° |
|---|---|---|
| 500 MHz | ±60 | ±65 |
| 600 MHz | ±60 | ±65 |
| 700 MHz | ±65 | ±65 |
| 800 MHz | ±65 | ±75 |
| 900 MHz | ±65 | ±75 |
| **Freq/Ele.** | **45°** | **90°** |
| 500 MHz | ±65 | / |
| 600 MHz | ±65 | / |
| 700 MHz | ±70 | / |
| 800 MHz | ±75 | / |
| 900 MHz | ±75 | / |

**TAB 5. Measured Beamwidth**

| Freq./Ele. | 0° | 20° |
|---|---|---|
| 500 MHz | ±70 | ±65 |
| 600 MHz | ±65 | ±65 |
| 700 MHz | ±60 | ±60 |
| 800 MHz | ±70 | ±60 |
| 900 MHz | ±80 | ±65 |
| **Freq/Ele.** | **45°** | **90°** |
| 500 MHz | ±55 | / |
| 600 MHz | ±65 | / |
| 700 MHz | ±65 | / |
| 800 MHz | ±100 | / |
| 900 MHz | ±100 | / |

### 6.3. Return Loss

The computation and measurement of the return loss reveals that increasing the frequency leads to enhanced accuracy. Although the simulation identifies three poles only the pole with the highest frequency can be modelled precisely. At lower frequencies the return loss is underestimated by the simulation because less reflections are obtained by the vector network analyzer. However a low return loss does not automatically refers to a high gain as seen in Table 3. According to MATLAB the mesh refines if the wavelength becomes shorter in order to obtain an accurate solution. This feature has been observed in form of longer simulation time for high frequencies. For this paper the mesh is automatically selected by MATLAB, no manual input is considered. It is recommended to apply manual meshing for thick dielectric according to the MATLAB manual [14].

### 6.4. Effect on Coverage Map

To study the effect of radiation pattern three different coverage maps are proposed. In case of the omnidirectional receiver no distinct lobes are observed hence all isolines are spaced equally. By taking the simulated pattern into account nulls and backlobes are observed. Although the gain becomes a function of azimuth, the coverage is mostly influenced at $\phi \gtrapprox \pm 150°$. Due to the large beamwidth of the LPDA the radiation pattern does not have a large impact on the receiving power for an low azimuth. Furthermore the effect of nulls can be observed in the measured coverage map. For certain directions the receiving power drops in a larger scale because of the extensive nulls. In addition back lobes can be clearly identified improving the probability of detection on the reverse side. The effects of side lobes or even grating lobes can increase in case of phased array antennas which outlines the necessity to consider radiation patterns in link budget analyses.

## 7. SUMMARY AND OUTLOOK

To evaluate the precision of numerical simulation of a LPDA fundamental parameters are derived at the beginning. Because of the previously proposed passive radar demonstrator and the appropriate toolbox, a LPDA is simulated and measured. A strategy to verify the performance is introduced, in addition the numerical and practical measurement is discussed in detail. Radiation patterns and return losses are obtained and applied to estimate the coverage of a passive radar. For particular angles sufficient results are obtained indicating that is modelled properly by the numerical simulation. Attention must be given to the nulls, which can deviate especially at high azimuth. The effect of deviations on the coverage is noticeable however only relevant at higher azimuth because of the present nulls. The correct mesh size is critical for the simulation model as seen in the analysis of the return loss. Inaccuracy of measurement cannot be excluded since the absorbent material is expected to degrade at lower frequencies. For future projects the time-domain far-field measurement can be investigated to improve the measurement period. Moreover different antennas types provided by the toolbox's catalog can be considered for further evaluations.

**Contact address:**

sergio.orasch@edu.fh-joanneum.at

## References

[1] Mark A. Richards, James A. Scheer, and William A. Holm. *Principles of Modern Radar - Vol. I: Basic Principles Vol. I: Basic Principle*. SciTech Publishing, 2010. ISBN: 978-1-891121-52-4.

[2] Klaus W. Kark. *Antennen und Strahlungsfelder - Elektromagnetische Wellen auf Leitungen, im Freiraum und ihre Abstrahlung*. Vieweg+Teubner Verlag, 2011. ISBN: 978-3-8348-1495-1.

[3] Constantine A. Balanis. *Antenna Theory - Analysis and Design*. John Wiley Sons, 2005. ISBN: 0-471-66782-X.

[4] IEEE Standard for Definitions of Terms for Antennas. *IEEE Std 145-2013 (Revision of IEEE Std 145-1993)*, pages 1–50, 2014. DOI: 10.1109/IEEESTD.2014.6758443.

[5] Heiner Kuschel, Diego Cristallini, and Karl Erik Olsen. Tutorial: Passive radar tutorial. *IEEE Aerospace and Electronic Systems Magazine*, 34(2):2–19, 2019. DOI: 10.1109/MAES.2018.160146.

[6] Karl Rothammel, Alois Krischke. *Rothammels Antennenbuch*. DARC Verlag, 2001. ISBN: 3-88692-033-X.

[7] Sergio Orasch, Flühr Holger. Aufbau und Evaluierung eines passiven Radarsensors auf Basis kommerzieller Hardware. *Deutsche Gesellschaft für Luft- und Raumfahrt - Lilienthal-Oberth e.V.*, 2022. DOI: 10.25967/570295.

[8] LD Systems. WS 100 DA. https://www.ld-systems.com/de/loesungen/dj-musiker/anwendungen/buehne/4713/ws-100-da, 2023. online, accessed 01.09.2023.

[9] The MathWorks Inc. Antenna Toolbox Documenation. https://de.mathworks.com/help/antenna/ug/method-of-moments-metal-and-dielectric.html, 2023. online, accessed 29.08.2023.

[10] Walton C. Gibson. *The Method of Moments in Electromagnetics*. Chapman Hall/CRC, 2008. ISBN: 978-1-4200-6145-1.

[11] Yi Huang, Kenneth Chan, and Barry Cheeseman. Review of broadband antenna measurements. In *2006 First European Conference on Antennas and Propagation*, pages 1–4, 2006. DOI: 10.1109/EUCAP.2006.4584706.

[12] Michael D. Foegelle. Antenna Pattern Measurement: Concepts and Techniques. *Compliance Engineering - Annual Reference Guide 2002*, 2002.

[13] Yi Huang, Tian H. Loh, Lars J. Foged, Yang Lu, Steve Boyes, and Hassan Chattha. Broadband antenna measurement comparisons. In *Proceedings of the Fourth European Conference on Antennas and Propagation*, pages 1–5, 2010.

[14] The MathWorks Inc. Antenna Toolbox Documenation. https://de.mathworks.com/help/antenna/ug/meshing.html, 2023. online, accessed 31.08.2023.